Defect engineered blue photoluminescence in ZnO:Al/TiO 2 heterostructures

C. Saini, S. Bhowmick, A. Barman, N. Kumar, A. Das, S. Khan, A. Claverie, D. Kanjilal, R. Mahato, K. Singh, et al.

Defect engineered blue photoluminescence in ZnO:Al/TiO_2 heterostructures

C. P. Saini, [1,2 *] S. Bhowmick,[2] A. Barman,[2] N. Kumar,[3] A. Das,[4] S. A. Khan,[3] A. Claverie,[5] D. Kanjilal,[3] R. N. Mahato[1], K. Singh[1] and A. Kanjilal[2]

[1]*School of Physical Sciences, Jawaharlal Nehru University, Delhi 110067, India*

[2]*Department of Physics, School of Natural Sciences, Shiv Nadar University, NH-91, Tehsil Dadri, Gautam Buddha Nagar, Uttar Pradesh 201 314, India*

[3]*Inter-University Accelerator Centre, Aruna Asaf Ali Marg, New Delhi 110 067, India*

[4]*Institute for Plasma Research, Atmospheric Plasma Division, Ahmedabad, Gujarat, India*

[5]*CEMES-CNRS and Université de Toulouse, 29 rue J. Marvig, 31055 Toulouse, France*

ABSTRACT

Tailoring the blue photoluminescence (PL) in Al-doped ZnO (AZO)/TiO_2 heterostructures is demonstrated by controlled induction of shallow defect centres by 50 keV Ar^+-ions. This is established by a combination of temperature dependent PL and electron paramagnetic resonance spectroscopy. The dominant blue-violet PL in as-grown sample comprises of a near band-edge emission, along with a peak associated with radiative recombination of the electrons in shallow donor levels (Zn interstitials) and the holes from the valence band. However, the evolution of an additional yellow-green PL band at a fluence of 1×10^{15} ions/cm^2 is governed by the deep donor levels, particularly ionized oxygen vacancies. The irradiation at 1×10^{16} ions/cm^2 further leads the formation of Zn vacancies (shallow acceptors) owing to the development of O-rich surface. The structural modifications of these samples have been investigated by FE-SEM, TEM, and Rutherford back-scattering. While small micro-cracks are found at a fluence of 2×10^{16} ions/cm^2, the formation of graded-layers is obtained at the highest fluence of 5×10^{16} ions/cm^2 owing to

ballistic intermixing and diffusion of the constituents. Detailed investigation suggests that a significant amount of Ti atoms is diffused in AZO by complete deterioration of the AZO/TiO_2 matrix at the highest fluence.

Keywords: Ion irradiation, transition metal oxides, heterostructure, photoluminescence, defects,

*Author to whom correspondence should be addressed; E-mail:
chetanprakashsaini11@gmail.com

INTRODUCTION

Successful fabrication of low dimensional transition metal oxide devices involves in-depth knowledge of defects, especially oxygen vacancies (V_o). Among various metal oxides, both Al-doped ZnO (AZO) and titanium oxide (TiO_2) are attractive candidates for exploring V_o for wide range of technological applications, such as light emitting diodes,[1-3] solar cells,[4-6] memory storage,[7,8] etc. In particular, the growth of an AZO film on TiO_2 leads to the formation of a type-II heterostructure owing to their close matching of bandgaps with an extraordinary charge separation capability by lowering recombination rate.[3,9] This bilayer structure is now considered to be promising even in the field of water splitting[10] and photocatalysis,[11] though the charge transport is significantly influenced by the point defects, especially at their interface. The chemical stability and the tolerance to nonstoichiometric phases of the individual material also make them flexible for tailoring interstitials/vacancies in a desired way without compromising the material properties. Previously we reported the role of V_o in nanostructured TiO_2 for controlling the functionality of the resistive switching devices,[12] and for tuning the wettability and optical bandgap.[13,14]

In case of nonstoichiometric ZnO (i.e. Zn-rich or O-rich ZnO), previous theoretical investigation revealed that the formation energy of defects, calculated as a function of respective Fermi level, usually dictates them to be charged.[15,16] However, it is difficult to precisely determine the formation energy of defects as the position of Fermi level in ZnO strongly depends on the doping type and its concentration.[16] For instance, in *n*-type ZnO, V_o and Zn interstitial (Zn_i) are deep and shallow donors and are having high formation energies, whereas Zn vacancies (V_{Zn}) are deep acceptors with low formation energies and in turn act as compensating centres.[15] Oba *et al.*[16] on the other hand, revealed that both V_o and Zn_i have very low formation energies

and thus serve as source of hole compensation centres in *p*-type ZnO, provided Fermi level is low.

In this context, photoluminescence (PL) spectroscopy is known to be a very sensitive and powerful technique to track the existence of defects in metal oxides like AZO and TiO_2, and to understand the nature of sub-band gap states generated either by perturbing the crystal structure,[17] doping with foreign elements,[18,19] or by directly introducing V_o and/or interstitials in the matrix.[20-22] For example, Lin *et al.* reported an intense blue and green, and faint yellow-orange luminescence band in ZnO nanostructures, and attributed this in the light of deep level defects,[20] particularly Zn_i, ionized V_o (V_o^+/V_o^{++}) and oxygen interstitials (O_i). In a similar fashion, anatase dominated TiO_2 nanostructures also provide a smooth PL signal, positioned at about 416 nm, where the involved mechanism is discussed in terms of the charge-transfer process from the conduction band to the localized self-trapped exciton states, in the presence of V_o.[21] Although previous studies have tried to understand the nature of defects and their corresponding impact on PL characteristics, detailed investigation of V_o and/or impurity driven localized electronic states in both TiO_2 and AZO, in conjunction with in-depth understanding of the PL properties of the AZO/TiO_2 heterostructure are still scarce. Using a bilayer structure adds more complexity, particularly at the interface due to the possible diffusion and intermixing of the constituent elements in each layer as a result of annealing or radiation exposure. In this respect, low-energy ion bombardment is an ubiquitous surface science technique due to its capability to control the evolution of V_o in a predetermined depth, and also their spatial distributions by proper selection of ion species, energy and fluence. Samples can be systematically examined by low temperature PL spectroscopy immediately after bombardment.

In this article, we report the impact of 50 keV Ar^+ ions in forming V_o in the AZO layer grown on top of a thin amorphous TiO_2 layer and their possible role behind the visible range PL emission at room temperature (RT). Further, temperature dependent PL analysis has been carried out in the range of 15 to 300 K to shed light on the involvement of ion beam induced defects, especially Zn_i and V_o. We also show the tolerance limit before reaching the extreme condition by developing micro-cracks via formation of voids and local evolution of a graded layer by heavy mixing of the constituent elements of AZO and TiO_2 films at a fluence of 5×10^{16} ions/cm^2. Such ion fluence dependent V_o and V_{Zn} in AZO/TiO_2 heterostructures have been found to be singly charged according to low temperature Electron Paramagnetic Resonance (EPR) study.

EXPERIMENTAL

About 10 nm thick amorphous TiO_2 layer was grown at RT on ultrasonically cleaned Si substrate (area 1×1 cm^2) by radio frequency (RF) magnetron sputtering (Excel Instruments) using a 100 W power supply. Highly pure (99.999%) oxygen and Ar gases were injected into the vacuum chamber (base pressure ~10^{-7} Torr) with a flow rate of 12 sccm and 30 sccm, respectively, to maintain the working pressure of 8 mTorr during deposition from a 2 inch diameter and 6 mm thick TiO_2 target (MTI corp., purity 99.99%). The substrate-to-target distance was kept at 13 cm with a substrate rotational speed of 9 rpm to have a uniform film thickness. Subsequently, about 95 nm thick AZO film was grown on TiO_2 at RT from a 2 inch diameter and 6 mm thick AZO target (MTI corp., purity 99.99%) by RF magnetron sputtering using 50 W power supply. Highly pure Ar gas (99.999%) was introduced into the vacuum chamber with a flow rate of 30 sccm, while the working pressure was maintained at ~5 mTorr during entire AZO deposition process. The substrate-to-target distance was kept at 8 cm and the

substrate rotational speed was 12 rpm. We should note here that TiO_2 and AZO have different sputtering yields, therefore growth parameters are optimized accordingly. Moreover, no post annealing or heat treatment was carried out on the AZO/TiO_2 samples. Following this AZO/TiO_2 heterostructures were bombarded eventually with 50 keV Ar^+-ions under normal incidence at RT (schematically shown in Fig. 1), keeping a constant beam current of ~1 μA and fluences in the range of $(0.1\text{-}5)\times10^{16}$ ions/cm^2.

The surface morphologies of the AZO/TiO_2/Si heterostructures have been studied before and after Ar^+-ion irradiation using field-emission scanning electron microscopy, FE-SEM (TESCAN MIRA-II). The chemical compositions and film thicknesses were extracted by analyzing the RBS (random) spectra, where the data were recorded by using 2 MeV He^+ ions produced by 1.7 MV Pelletron accelerator at the Inter-University Accelerator Centre (IUAC), New Delhi. The visible range PL measurements were performed in the temperature range of 15–300 K by mounting the sample in a closed-cycle helium cryostat, while the samples were excited by a 30 mW He-Cd laser (325 nm wavelength). Moreover, ion beam irradiation induced structural evolution along with intermixing of bilayer films were examined by cross-sectional TEM (XTEM) using a Tecnai FEI (Cs corrected). Here, all TEM specimens were prepared by Focused Ion Beam (FIB Helios dual beam) after depositing a Pt layer on the sample surface in order to protect the top surface. In addition, EPR experiments were carried out at the Dresden High Magnetic Field Laboratory (Hochfeld-Magnetlabor Dresden, HLD) of Helmholtz-Zentrum Dresden-Rossendorf (HZDR) with the help of an X-band "Bruker Elexsys E500" EPR spectrometer operating in the range of 9.35 to 9.40 GHz and equipped with "Oxford Instruments" helium-4 flow-type cryostat with a lowest accessible temperature of ~2 K. The data were recorded for a microwave power of 1 mW and 5 Oe field modulation amplitude.

RESULTS AND DISCUSSION

Prior to Ar^+-ion exposure, the penetration depth of ions and vacancy distribution were estimated by Stopping and Range of Ions in Matter (SRIM 2013) calculations.[23] A typical depth dependent vacancy distributions profile in AZO film is shown in Fig. 2, revealing the formation of both Zn and O vacancies within 80 nm and dominance in the range of 20–30 nm from the surface.

Typical plan-view FE-SEM image of as-grown AZO/TiO_2 heterostructure is displayed in Fig. 3(a), showing that the AZO surface is made of small grains with an average diameter of ~15 nm. Further, 50 keV Ar^+-ion bombardment leads to the gradual increase in roughness. Micro-cracks which are visible after irradiation with a fluence of 1×10^{16} ions/cm^2 [Fig. 3(b)] are found to be transformed to a wrinkle-like pattern at a fluence of 2×10^{16} ions/cm^2 [Fig. 3(c)]. Further increase in ion fluence up to 5×10^{16} ions/cm^2 leads to complete deterioration of the AZO/TiO_2 heterostructure owing to preferential sputtering of surface atoms followed by the formation of large voids (70–80 nm in diameter) in Si substrate, as evidenced from Fig. 3(d).

For microstructural investigation of AZO/TiO_2 structure with increasing ion fluence, detailed XTEM have been carried out of some selected samples. As can be seen in fig. 4 (a), low magnification XTEM of as-grown AZO/TiO_2/Si sample revealed the smooth and conformal growth of AZO film which is located in between the Si substrate and Pt layer though it's hardly shows any signature of TiO_2 film owing to very low thickness. We should note here that a thin Pt layer was grown prior to TEM sample preparation for protecting the top surface of AZO. The average thickness of AZO film, measured by imageJ software using spectra is found to be around ~102 nm. However, high resolution TEM (HRTEM) image of dashed circular region [Fig. 4 (b)]

not only confirms the crystalline nature of the AZO film but also clearly evident the existence of thin amorphous TiO_2 film with average thickness of 10 nm. Closed inspection, further confirmed the formation of very thin (4.5 ± 0.5 nm) native oxide SiOx layer at the TiO_2/Si interface which originated due to the diffusion of oxygen radicals during the growth of TiO_2 film.

Moreover, the XTEM image of the AZO/TiO_2 heterostructure after bombarding with a fluence of 1×10^{16} ions/cm^2 is displayed in Fig 4(c), indicating a significant reduction in AZO film thickness (~92 nm) due to sputtering of AZO layer. Close inspection further revealed a surprising enhancement in the underneath TiO_2 thickness from ~10 to 14 nm [see Fig. 4(d)]. We believe that this could be due to ion beam induced swelling of the TiO_2 film because of out-diffusion of oxygen atoms from the native oxide layer for reducing the difference in chemical potential at their interfaces.

Further increase in ion fluence up to 5×10^{16} ions/cm^2 leads to complete degradation of the AZO/TiO_2 matrix in conjunction with evolution of voids [see Fig. 4(e)]. This is clearly visible in HRTEM spectra as shown by Fig. 4(f), acquired at dashed circle in Fig. 4(e), indicating the formation of bigger voids within the range of 40-50 nm along with small ones. This is consistent with our SEM results. In particular, the evolution of such bigger voids can be results the coalescence of smaller ones bombarded at a fluence of 5×10^{16} ions/cm^2. In addition, ion irradiation causes the intermixing of AZO and TiO_2 layers by formation of Ti, Zn and O rich graded layers and reduction in overall film thickness of 65 ± 5 nm though its not uniform throughout the surface. [see Figs. 4 (f)]. Close inspection of the spectra further revealed the evolution of amorphous layer near the surface of Si substrate, enriched with O up to a depth of ~52 ± 2 nm from the surface.

In order to study the modification of average thickness, atomic density, and chemical composition of the bilayer structure, RBS spectra were recorded before and after ion beam exposure, as exhibited in Fig. 5. The chemical composition of the films and (areal) atomic densities of the constituent elements were extracted by fitting the RBS spectra using Rump software[24] (shown in Fig. 6), where the values are summarized in Tables I and II, respectively. As discerned from Fig. 5, the Si edge was clearly shifted towards higher channel number with increasing ion fluence and it became severe at 5×10^{16} ions/cm^2 (shown by dashed arrow). Close inspection suggests a gradual reduction of the Zn and Ti peak intensities in conjunction with a shift in Ti edge towards higher channel numbers, especially above a critical fluence of 1×10^{16} ions/cm^2. The shift of Ti peak towards Zn is equally related to the increasing growth of SiOx layer on Si substrate. This could be a signature of the systematic reduction of average film thickness of AZO from its initial value of ~101 nm to ~90 nm (using average density of 7.3 × 10^{22} atoms/cm^3) due to sputtering loss of Zn and O atoms from the surface, in parallel to interfacial mixing of the TiO_2 film with increasing ion fluence up to 2×10^{16} ions/cm^2 consistent with our XRTEM results. This is though not applicable for 5×10^{16} ions/cm^2 fluence as the AZO/TiO_2 heterostructure was found to be entirely degraded [see Fig. 4(f) for clarity]. However, this effect is not that prominent up to a fluence of 1×10^{16} ions/cm^2 owing to the relatively high bonding/cohesive energy of O in TiO_2 (-9.79 eV) than that of ZnO (-7.52 eV),[25,26] and also for having almost 10 times large ZnO film thickness with respect to TiO_2. Indeed, the observed broadening of the Ti peak at 5×10^{16} ions/cm^2 can be explained in the light of the diffusion of segregated Ti into the remaining AZO. In order to understand the phenomenon, it is now important to check the oxygen edge with increasing ion fluence, though it is clear in Fig. 6. As discerned from Fig. 6(a), the O signals from the AZO and TiO_2 films are overlapped in the RBS

random spectrum and thus provide a broad O peak, though the contribution is more from the AZO film because of higher thickness. We cannot however neglect the contribution of oxygen present in the natural oxide layer on Si substrate. Interestingly, the oxygen peak width is found to decrease gradually with increasing fluence, especially above 1×10^{16} ions/cm^2 [see Figs. 6(b)–(d)], and this can be attributed to the decreasing thicknesses of the oxide layers by ion beam sputtering loss of atoms from the AZO surface region. Since the oxide signal in the lower channel region is mainly lost due to the increasing fluence (Fig. 5), it is clear that the oxygen from TiO_2 film is equally sputtered with AZO when the energetic Ar^+ ions can reach there above a fluence of 1×10^{16} ions/cm^2. Although ion implantation leads to modification in film stoichiometry, the variation in areal density of elements before and after ion exposure is however modest (see Table II). Beside this, the signature of Ar implanted atoms has also been witnessed with increasing ion fluence (see Table II), leading to the evolution of Ar peak at 2×10^{16} ions/cm^2 [Fig. 6(c)] and further intensified at 5×10^{16} ions/cm^2, as revealed from Fig. 6(d). Comparing the atomic density of Ar in the samples irradiated with fluences of 2×10^{16} and 5×10^{16} ions/cm^2, one can see that almost a factor of 4 numbers of Ar atoms were lost in the former case. However, the intensity of the sharp Si edge remains unaffected.

The RBS results are found to be consistent with the corresponding cross-sectional TEM (XTEM) results showing a decrease of the initial AZO film thickness by ~10 nm at a fluence of 1×10^{16} ions/cm^2 in the presence of Ar. Figure 6(b) also suggests that the Ar atoms are mostly confined within the heterostructure at this fluence. Given the existence of Ar within the Si substrate [see Figs. 6(c) and (d)] indicates a significant reduction of the combined film thickness at a fluence of 2×10^{16} ions/cm^2, followed by a complete degradation of the AZO/TiO_2 heterostructure at 5×10^{16} ions/cm^2 good agreement with our XRTEM results.

Since the fitting program RUPM involves two important parameters like the interface position and its standard deviation (σ), the knowledge of variance of the second component, say surface roughness (σ_s) and the interfacial concentration gradient (σ_i), is very important for proper understanding, details can be found in References.[27,28] In the present bilayer structure, as we have seen the evolution wrinkle-like features at surface [see Fig. 3(c)], the effect of σ_s cannot be neglected in the present fitting process for 2×10^{16} ions/cm^2. This is equally applied for 5×10^{16} ions/cm^2 due to the formation of clusters on the Si substrate with void–like structures [see Fig. 3(d) for clarity]. Considering the XTEM results, it is clear that the RUMP fitting in Fig. 5(d) has been affected not only by the surface roughness, but also by the mixed film/Si interface, especially the formation of a thick and uneven interfacial SiO_x layer beside the development of voids and rough Si surface. We believe that the increase in interfacial SiO_x layer with uneven Si surface has strong impact on the Si edge beyond the critical fluence of 1×10^{16} ions/cm^2, as evident from Fig. 5. Since the fitting the ballistic mixing effect in RBS spectra are very much dictated by the atomic density, stopping power employed for Si and residual channeling in Si substrate etc. Here we have enlisted the areal atomic densities of the constituent atoms have been determined for four different samples (see Table II).

As can be seen from Table I, as-grown AZO film exhibits relatively higher Zn concentration than that of O, showing the stoichiometry imbalance in the as-grown sample. This stoichiometry imbalance could be due to lack of O incorporation during the growth of AZO films, leading to the formation of O deficient AZO films. On the other hand, the increase in ion fluence apparently gives rise to a decrease in overall Zn concentration, consistent with our Energy Dispersive X-ray Spectroscopy (EDS) results (not shown). This stoichiometric restoration may appear from the preferential sputtering of Zn atoms from the surface (owing to

the lower surface binding energy of Zn, compared to that of O) and diffusion, and readjustment of O atoms. Further increase of fluence up to 5×10^{16} ions/cm^2 causes the complete deterioration of the AZO/TiO_2 interface via intermixing of constituent elements, which in turn leads to the formation of a single graded layer structures (see Table II).

Typical temperature dependent PL (~15–300 K) spectra of the as-grown AZO/TiO_2 heterostructure are displayed in Fig. 7(a). Since the penetration depth of He-Cd laser (325 nm wavelength) in ZnO is limited to 50-80 nm,[29] the majority of optical absorbance and consequent photoexcitation occur within the AZO layer of heterostructure. Since our XRTEM results clearly demonstrated that the underneath TiO_2 layer was amorphous in nature, the observed PL mainly originates from the AZO film. It appears that the spectrum consists of at least five components (indicated by 1 to 5), and the peak intensity increases systematically with decreasing *T* down to 15 K, where all associated peaks are well resolved and distinguishable. Close inspection further reveals a broad visible range hump in the as-grown sample at RT, and it is attributed to the dominance of defect-related luminescent centers (LCs), especially V_o and interstitials in AZO,[30,31] though no signature of band-edge emission was recorded. By lowering the temperature, the gradual increase in PL intensity was observed, which is mainly attributed to reduction of the non-radiative de-excitation channels, frizzing-out phonons and concentration reduction of free carriers in the conduction band (CB).[32] In particular, the peak 1, detected at the emission wavelength of ~378 nm (3.28 eV) was found to be blue shifted continuously with lowering T, whereas peak 2, detected at ~397 nm (3.12 eV), was slightly blue shifted only at lowest T (15 K). In fact, peak-1 is attributed to near band-edge (NBE) emission whereas Peak-2 is likely to be associated with the transition from neutral donor-bound exciton, free exciton and/or donor to acceptor pair.[33-37] Although no discernible change in position of peak 3 and 4 was found with

decreasing T, the position of peak 5 however shifted towards higher wavelength region (see dashed line of peak 5) with decreasing T. These peaks are mainly associated with defect related LCs arises within the bandgap; details can be found in Refs. [9,30,38,39] Here, the 3–5 PL peaks are found to be at ~420 (2.95 eV), 434 (2.85 eV) and 460 nm (2.69 eV), in the blue-violet region, but their origin and mechanism are still controversial.[9,38] For instance, Zeng *et al.* have shown that violet emission in ZnO can be attributed to the electron transition from shallow donor states, located at ~0.22 eV below the CB, to the valence band (VB) and related to the neutral Zn_i interstitial (Zn_i^*), whereas transitions from ionized Zn_i interstitials(Zn_i^+ and/or Zn_i^{++}) of slightly lower energies than Zn_i^* (~0.54 to ~0.65 eV below the CB) are responsible for the blue emission.[40] In fact, the probability of formation of Zn_i interstitials is significantly higher in as-grown AZO film owing to have relatively high Zn concentration, in consistent with the RBS (see Table I). It is worth to note that Zn_i^* is formed in ZnO due to the formation of a Frenkel pair through atomic collisions ($Zn_{Zn} \leftrightarrow Zn_i^* + V_{Zn}^*$) which are further ionized ($Zn_i^* \leftrightarrow Zn_i^+ + e^-$ and $Zn_i^+ \leftrightarrow Zn_i^{++} + e^-$) and finally lead to the formation of extended Zn_i interstitial states.[41] In contrast, Peng *et al.* have shown that the band bending found in ZnO grains can result electron depletion in the regions where electron transition from the CB to defect levels located inside the depletion regions (~0.7 eV above the VB) governs the blue emission.[39] A schematic representation of all these proposed defect related PL emissions in AZO is shown in Fig. 7(e).

On the other hand, the PL spectrum of the sample implanted with a fluence of 1×10^{15} ions/cm^2 (see Figure 7(b)) is clearly different from the one obtained in as-grown sample, especially at the longer wavelength region. In particular, the broad hump which appears in the range of 450-600 nm, in the green-yellow-orange band, (indicated by an arrow on peak-3) becomes even more prominent at low T (15 K). It is attributed to the radiative recombination of charge carriers from

the CB to deep acceptors like oxygen interstitials or associated to ionized V_o in AZO matrix.[20,30,31] In particular, green luminescence is attributed to the transition of electrons from neutral or singly ionized V_o (located 0.8–1.0 eV below the CB minima) to the VB edge whereas the transitions from CB to oxygen interstitials and doubly ionized V_o are responsible for yellow and orange emissions.[20,30] Lin *et.al.* has shown that yellow luminescence in ZnO is associated to the band-acceptor transition and further red shifted with decreasing temperature.[20] Interestingly, unlike what is observed in the as-grown sample, the NBE of AZO as shown by dashed line of peak-1 in Fig. 7(a) has completely disappeared. The quenching of such NBE is also previously reported and attributed to the defects like vacancies in Zinc sublattice which may evolve here during ion irradiation and eventually acts as trapping sites.[42] On the other hand, the LCs related violet emission, centered at ~402 and ~421 nm, are still visible and are indicated by peaks-1 and 2, respectively. The origin of the emission at ~421 nm seems to be understood (discussed above), but the mechanism behind the PL emission found at ~402 nm is still controversial, although sometimes associated with the donor-acceptor pair with longitudinal optical (LO) phonon replicas.[39] The trend was confirmed when observing the spectrum obtained on the sample bombarded with a fluence of 1×10^{16} ions/cm^2. This time, peak-2 (~421 nm) is slightly blue shifted as evidenced in Fig. 7(c). Such blue shifting suggests some alteration of the environment or the nature of defect responsible for this emission, probably by the formation of shallow acceptors like V_{Zn} with different charge states.[40] In fact, irradiation with a fluence of 1×10^{16} ions/cm^2 causes the preferential surface sputtering of the Zn atoms, leading to the reduction of the relative concentration of Zn (see Table I) and in turn promote the formation of V_{Zn}. Further increase of the ion fluence (i.e. 5×10^{16} ions/cm^2) leads to some dramatic change in the PL spectrum, which can be ascribed to the strong intermixing of the AZO/TiO_2/Si structure and the

formation of voids as seen in Fig. 7(d). Interestingly, no PL signal was detected at RT on this sample and this could result from the dominance of phonons in this structure. In fact, it follows a similar trend in the as-grown sample below 250 K. As can be seen, peaks-1 in Fig. 7(a), which are assigned to near band-edge emission of AZO, was dramatically evolved again [see peak 1 in Fig 7(d)] where the intensity of peak-2 is significantly higher, unlike as-grown one. Close inspection further revealed that the peak-3 centered around blue region is driven by the ionized V_{Zn}, and it is well resolved and intense, suggesting more localization of the defect states around V_{Zn}.

Since low temperature (2.2 K) EPR spectroscopy is highly sensitive to paramagnetic species containing unpaired electrons,[43] we have used this technique for investigating the defects in the AZO/TiO_2 structure. As seen in Fig 8(a), all samples show symmetrical EPR signals at around g~2.002, suggesting the existence of the same type of paramagnetic centers in all samples. It is worth here to note that the intensity of each spectrum was normalized by taking into account the sample size and layer thicknesses. In previous studies, paramagnetic defects in ZnO were controversially discussed in the light of singly charged vacancies, such as $V_o^+$and V_{Zn}^-.[38,44-46] In fact, $V_o^+$and V_{Zn}^- (generated by trapping of one electron from the conduction band and consequently positively charged with respect to lattice) were previously considered as shallow acceptor and deep donor defects, respectively.[38,46-48] In the as-grown sample, the existence of V_{Zn}^- in ZnO is significantly less probable (due to relatively smaller density) owing to its larger defect formation energy (~4 eV) than V_o^+ and therefore discarded. Previous EPR studies on ZnO have shown that V_o^+ has tendency to localized on the surface region of ZnO which in turn results the EPR signal at g = ~2.004.[49,50] As can be seen from Fig. 7 (a), the value of g-factor is very close in all as-grown as well as irradiated samples and matches well with g-factor of free electron (g_e =

~2.0023), indicating the delocalization of surface defects.[51] Beside this, other defect states like doubly ionized V_o (V_o^{++}), Zn and O in interstitial site (i.e., Zn_i and O_i^{2-}) could also be formed with ion irradiation and may coexist with the paramagnetic defects (V_{Zn}^{-} and/or V_o^{+}) found in the AZO layer. However, it is difficult to detect these defects with EPR as they are diamagnetic in nature.[38] Nevertheless, displacement of the Zn and O atoms from their regular lattice sites leads to the possible formation of singly ionized vacancies, where the concentration increases further under the exposure of energetic Ar^+ ions. Moreover, linewidth of the EPR signals is enhanced from ~1.20 to ~1.31 mT by exposing to an ion fluence of 1×10^{16} ions/cm^2, but is decreased to ~1.14 mT at an ion fluence of 5×10^{16} ions/cm^2 [see Fig. 8(b)]. The EPR linewidth depends generally on the spin-lattice and spin-spin interactions of unpaired electrons, while the latter one dominates more. In fact, a spin-spin interaction is related with mutual spin flips resulted by dipolar and exchange interactions between assembly of spins in the sample.[52] Here, the initial increase in EPR linewidth can be attributed to the increase in strain within the layer and to its effect on the crystalline environment of the defect centers. With further increase in ion fluence, the decrease in EPR linewidth is most likely associated with the reduction of heterogeneous distribution of V_o^{+} centers by suppressing strain via evolution of voids as evidenced by FE-SEM and TEM results and so the effect on g tensor.[14]

CONCLUSIONS

In conclusion, we report a compositional variation and the subsequent change of defects in AZO/TiO_2 heterostructures by exposing to 50 keV Ar^+ ions. We have correlated these defects to the observed PL in the region of visible range as a function of temperature. As-grown AZO layer on TiO_2/Si surface initially provides an emission peak in the blue-violet region, which is attributed to the transition of electrons from the near band edge and Zn interstitials to the valence

band. An additional broad PL band in the green-yellow region (450-600 nm) is evidenced at a fluence of 1×10^{15} ions/cm^2 owing to active participation of deep donors originated from the ionized V_o. Further increase in ion fluence led to the formation of microcracks with gradual reduction in Zn concentration via preferential surface sputtering of Zn atoms, suggesting the evolution of V_{Zn} in AZO layer. The highest fluence of 5×10^{16} ions/cm^2 causes a complete deterioration of the AZO/TiO_2 bilayer structure by intermixing of the constituent elements and evolution of voids which eventually leads to the formation of the chemically graded intermediate layer.

ACKNOWLEDGEMENTS

CPS would like to acknowledge the financial support received from the Dr. D. S. Kothari Postdoctoral fellowship (F.4-2/2006(BSR)/PH/19–20/0074), UGC. AK would like to acknowledge the financial support received from Shiv Nadar University. The help received from the scientists at Inter-University Accelerator Centre is highly acknowledged. Authors are also grateful to Dr. S. Zvyagin (High magnetic field laboratory) and Dr. S. Prucnal (Institute of Ion Beam Physics and Materials Research) form HZDR for performing the EPR and low temperature PL experiments, respectively. One of authors (DK) is thankful to Department of Atomic Energy for awarding Raja Ramanna fellowship.

References

[1] D. Yan, W. Zhang, J. Cen, E. Stavitski, J.T. Sadowski, E. Vescovo, A. Walter, K. Attenkofer, D.J. Stacchiola, M. Liu, Appl. Phys. Lett., 111 (2017) 231901.

[2] Y.-S. Lin, Y.-H. Huang, W.-C. Huang, Vacuum, 122 (2015) 143-146.

[3] E. G-Berasategui, C. Zubizarreta, L. Mendizabal, J. Barriga, A. Viñuales, J. Palenzuela, Y. Alesanco, B. Herbig, U. Posset, Vacuum, 151 (2018) 108-115.

[4] M.-T. Tsai, Z.-P. Yang, T.-S. Jing, H.-H. Hsieh, Y.-C. Yao, T.-Y. Lin, Y.-F. Chen, Y.-J. Lee, Solar Ener. Mater. Solar Cells, 136 (2015) 17-24.

[5] S. Feng, P. lv, D. Ding, R. A, T. Liu, P. Su, W. Yang, J. Yang, W. Fu, H. Yang, Vacuum, 166 (2019) 255-263.

[6] X. Wang, H. Guo, C. Ma, X. Jia, Y. Li, N. Yuan, J. Ding, Vacuum, 166 (2019) 201-205.

[7] A. Kumar, M. Das, V. Garg, B.S. Sengar, M.T. Htay, S. Kumar, A. Kranti, S. Mukherjee, Appl. Phys. Lett., 110 (2017) 253509.

[8] S. Wan, Y. Yan, C. Wang, Z. Yang, J. Zhao, Vacuum, 156 (2018) 91-96.

[9] L. Pan, G.-Q. Shen, J.-W. Zhang, X.-C. Wei, L. Wang, J.-J. Zou, X. Zhang, Indus. Engin. Chem. Res., 54 (2015) 7226-7232.

[10] Y. Mi, L. Wen, R. Xu, Z. Wang, D. Cao, Y. Fang, Y. Lei, Advan. Ener. Mater., 6 (2015) 1501496.

[11] X.W. Zhang, C.C. Liu, G.R. Han, Materials Science Forum, Trans Tech Publ, 2009, pp. 707-710.

[12] A. Barman, C.P. Saini, P.K. Sarkar, A. Roy, B. Satpati, D. Kanjilal, S.K. Ghosh, S. Dhar, A. Kanjilal, Appl. Phys. Lett., 108 (2016) 244104.

[13] C.P. Saini, A. Barman, B. Satpati, S.R. Bhattacharyya, D. Kanjilal, A. Kanjilal, Appl. Phys. Lett., 108 (2016) 011907.

[14] C.P. Saini, A. Barman, D. Das, B. Satpati, S.R. Bhattacharyya, D. Kanjilal, A. Ponomaryov, S. Zvyagin, A. Kanjilal, J. Phys. Chem. C, 121 (2017) 278-283.

[15] A. Janotti, C.G. Van de Walle, Phys. Rev. B, 76 (2007) 165202.

[16] F. Oba, M. Choi, A. Togo, I. Tanaka, Sci. Tech. Adv. Mater., 12 (2011) 034302.

[17] M. Biswas, Y.S. Jung, H.K. Kim, K. Kumar, G.J. Hughes, S. Newcomb, M.O. Henry, E. McGlynn, Phys. Rev. B, 83 (2011) 235320.

[18] Z. Ahmed Khan, A. Rai, S. Roy Barman, S. Ghosh, Appl. Phys. Lett., 102 (2013) 022105.

[19] K.-W. Seo, H.-S. Shin, J.-H. Lee, K.-B. Chung, H.-K. Kim, Vacuum, 101 (2014) 250-256.

[20] Y.-J. Lin, C.-L. Tsai, Y.-M. Lu, C.-J. Liu, J. Appl. Phys., 99 (2006) 093501.

[21] C.P. Saini, A. Barman, D. Banerjee, O. Grynko, S. Prucnal, M. Gupta, D.M. Phase, A.K. Sinha, D. Kanjilal, W. Skorupa, A. Kanjilal, J. Phys. Chem. C, 121 (2017) 11448-11454.

[22] F. Tariq, N.u. Rehman, N. Akhtar, R.E. George, Y. Khan, S.u. Rahman, Vacuum, 171 (2020) 108999.

[23] J.F. Ziegler, M.D. Ziegler, J.P. Biersack, Nucl. Instrum. and Methods B, 268 (2010) 1818-1823.

[24] L.R. Doolittle, Nucl. Ins. and Methods Phys. Res. Sec. B: Beam Inter. Mater. and Atoms, 9 (1985) 344-351.

[25] N.I. Medvedeva, V.P. Zhukov, M.Y. Khodos, V.A. Gubanov, phys. status solidi (b), 160 (1990) 517-527.

[26] Ü. Özgür, Y.I. Alivov, C. Liu, A. Teke, M.A. Reshchikov, S. Doğan, V. Avrutin, S.-J. Cho, H. Morkoç, J. Appl. Phys., 98 (2005) 041301.

[27] A. Crespo-Sosa, P. Schaaf, W. Bolse, K.-P. Lieb, M. Gimbel, U. Geyer, C. Tosello, Phys. Rev. B, 53 (1996) 14795-14805.

[28] N.-T. Kim-Ngan, A. Balogh, J. Brötz, M. Zajac, J. Korecki, Acta Phys. Polonica, A., 118 (2010).

[29] A.-S. Gadallah, M.M. El-Nahass, Advan. Conden. Matter Phys., 2013 (2013) 11.

[30] T. Dixit, I. Palani, V. Singh, J. Phys. Chem. C, 121 (2017) 3540-3548.

[31] T. Dixit, A. Bilgaiyan, I.A. Palani, D. Nakamura, T. Okada, V. Singh, J. Sol-Gel Sci. Tech., 75 (2015) 693-702.

[32] D.W. Hamby, D.A. Lucca, M.J. Klopfstein, G. Cantwell, J. Appl. Phys., 93 (2003) 3214-3217.

[33] S. Prucnal, J. Wu, Y. Berencén, M.O. Liedke, A. Wagner, F. Liu, M. Wang, L. Rebohle, S. Zhou, H. Cai, W. Skorupa, J. Appl. Phy., 122 (2017) 035303.

[34] S. Repp, S. Weber, E. Erdem, J. Phys. Chem. C, 120 (2016) 25124-25130.

[35] K.P. O'Donnell, X. Chen, Appl. Phys. Lett., 58 (1991) 2924-2926.

[36] T. Basu, M. Kumar, S. Nandy, B. Satpati, C.P. Saini, A. Kanjilal, T. Som, J. Appl. Phys. 118 (2015) 104903.

[37] E. Sonmez, S. Aydin, M. Yilmaz, M.T. Yurtcan, T. Karacali, M. Ertugrul, J. Nanomaterials, 2012 (2012) 3-3.

[38] H. Kaftelen, K. Ocakoglu, R. Thomann, S. Tu, S. Weber, E. Erdem, Phys. Rev. B, 86 (2012) 014113.

[39] Y.-Y. Peng, T.-E. Hsieh, C.-H. Hsu, White-light emitting ZnO–SiO_2 Nanotechnology, 17 (2005) 174.

[40] H. Zeng, G. Duan, Y. Li, S. Yang, X. Xu, W. Cai, Advan. Funct. Mater., 20 (2010) 561-572.

[41] F. Kayaci, S. Vempati, I. Donmez, N. Biyikli, T. Uyar, Nanoscale, 6 (2014) 10224-10234.

[42] J. Piqueras, E. Kubalek, Phys. Status Solidi (a), 91 (1985) 569

[43] T. Su, Y. Yang, Y. Na, R. Fan, L. Li, L. Wei, B. Yang, W. Cao, ACS Appl. Mater. & Inter., 7 (2015) 3754-3763.

[44] D. Galland, A. Herve, Phys. Lett. A, 33 (1970) 1-2.

[45] A.L. Taylor, G. Filipovich, G.K. Lindeberg, Solid State Commun., 8 (1970) 1359-1361.

[46] L. Zhang, L. Yin, C. Wang, N. lun, Y. Qi, D. Xiang, J. Phys. Chem. C, 114 (2010) 9651-9658.

[47] J.r.J. Schneider, R.C. Hoffmann, J.r. Engstler, A. Klyszcz, E. Erdem, P. Jakes, R.d.-A. Eichel, L. Pitta-Bauermann, J. Bill, Chem. Mater., 22 (2010) 2203-2212.

[48] R. Baraki, P. Zierep, E. Erdem, S. Weber, T. Granzow, J. Phys: Condens Matter, 26 (2014), 115801.

[49] S. Nadupalli, S. Repp, S. Weber, E. Erdem, Nanoscale, 13 (2021) 9160.

[50] M. B.-Akturk, M. Toufani, A. Tufani, E. Erdem, Nanoscale, 14 (2022) 3269.

[51] A.U. Ammar, I.D. Yildirim, F. Bakan, E. Erdem, Beilstein J. Nanotechnol, 12 (2021) 49-57.

[52] D.M. Murphy, ChemInform, 41 (2010) 1-10

Figure Captions

FIG. 1 Schematic representation of the 50 keV Ar^+-ion exposure to AZO/TiO_2 heterostructure on Si

FIG. 2 SRIM calculation for 50 keV Ar^+-ions in AZO film showing the distribution of Zn, O and Al vacancies per ion with penetration depth, where '0' depth represents the sample surface.

FIG. 3 Typical plan-view FE-SEM image of AZO/TiO_2 heterostructures on Si for (a) as-grown, and after bombarding with 50 keV Ar^+ ions for fluences of (b) 1×10^{16}, (c) 2×10^{16} and (d) 5×10^{16} ions/cm^2.

FIG. 4 (a) XTEM image of as-grown sample, (b) HRTEM image of white dashed circle region in (a). whereas XTEM and corresponding HRTEM image of Ar^+ ion irradiated samples at a ion fluence of 1×10^{16} ions/cm^2 and of 5×10^{16} ions/cm^2 are shown by (c),(d) (e) and (f), respectively.

FIG. 5 RBS spectra of the AZO/TiO_2 heterostructures before and after 50 keV Ar^+-ion irradiation.

FIG. 6 Experimental data of RBS (black curve) and the corresponding simulated spectra (red curve) of AZO/TiO_2 heterostructures on Si are shown for (a) as-grown, and after bombarding with 50 keV Ar^+-ions with fluences of (b) 1×10^{16} ions/cm^2, (c) 2×10^{16} ions/cm^2, and (d) 5×10^{16} ions/cm^2, respectively.

FIG. 7 Temperature dependent PL spectra of AZO/TiO_2 hetrostructure for (a) as-grown and the Ar^+-ion exposed samples with fluences of (b) 1×10^{15}, (c) 1×10^{16} and (d) 5×10^{16} respectively. The corresponding schematic band diagram with various defect related energy states in ZnO are exhibit in (e).

FIG. 8 (a) Low temperature (2 K) EPR spectra of before and after ion exposure with fluences of 1×10^{16} and 5×10^{16} ions/cm^2. The intensity of each spectrum was normalized by taking into account the sample size and layer thickness. Variation of the corresponding EPR linewidth as a function of ion fluence is shown in (b).

Table I: Ar^+ ion induced thickness and compositional variation of the AZO/TiO_2 heterostructures, extracted by fitting the RBS spectra using of RUMP software.

Layer composition	Element(s)	Atomic percentage (±0.3 at.%) for samples			
		As-grown	Irradiated with 1×10^{16} ions/cm^2	Irradiated with 2×10^{16} ions/cm^2	Irradiated with 5×10^{16} ions/cm^2
TiO_2	Ti	50	31.6	24.2	13.4
	O	50	68.4	75.8	-
AZO	Zn	54.5	50.5	47.4	28.9
	O	43.5	45.5	46.3	45.3
	Al	2	2	2.1	2.1
	Ar	0	2	4.2	10.3

Table II: AZO film thickness and the corresponding areal density of the constituent elements with increasing ion fluence, extracted by RUMP software.

Samples irradiated with fluence (ions/cm^2)	AZO Thickness (nm ± 3 nm)	Areal density (atoms/cm^2)			
		Ti	O	Zn	Ar
0	101	6.04×10^{16}	5.32×10^{18}	4.45×10^{17}	0
1×10^{16}	95	5.54×10^{16}	5.25×10^{18}	3.95×10^{17}	-
2×10^{16}	90	5.37×10^{16}	5.12×10^{18}	2.93×10^{17}	5.25×10^{15}
5×10^{16}	65 (graded structures)	5.15×10^{16}	3.40×10^{18}	9.63×10^{16}	3.37×10^{16}

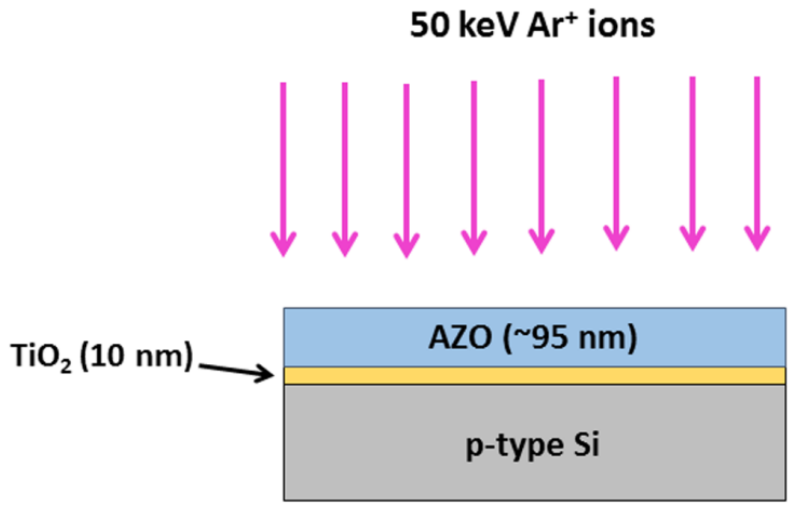

FIG. 1. Saini *et al.*

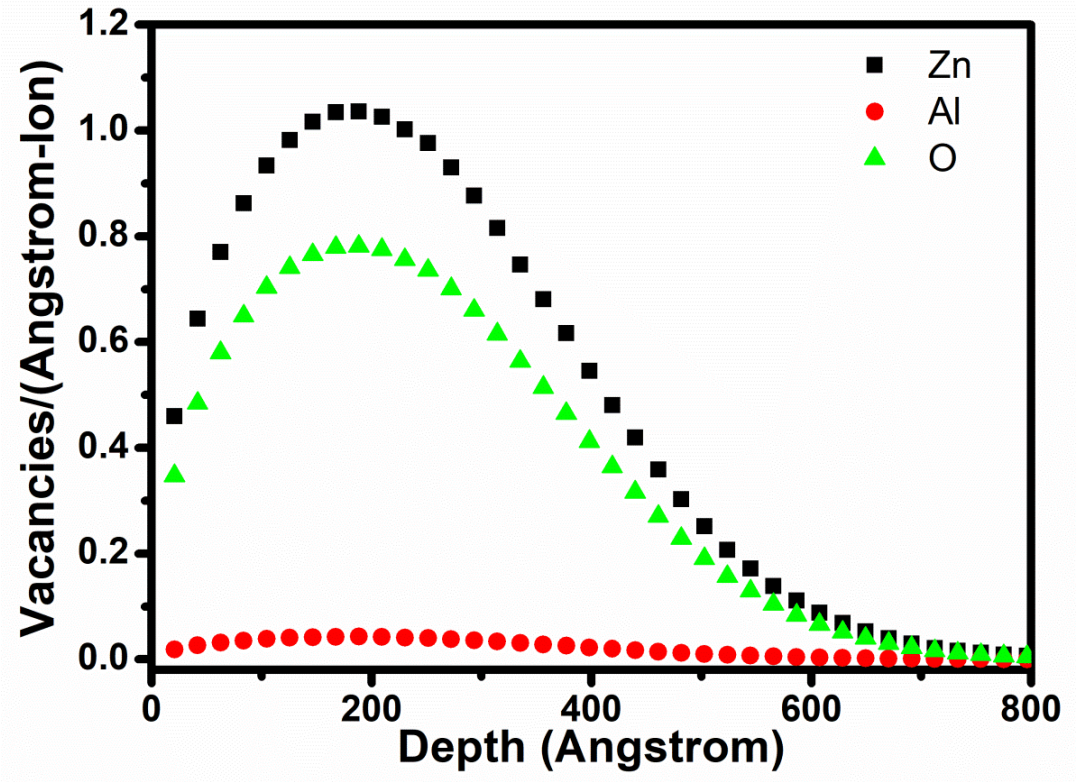

FIG. 2. Saini *et al.*

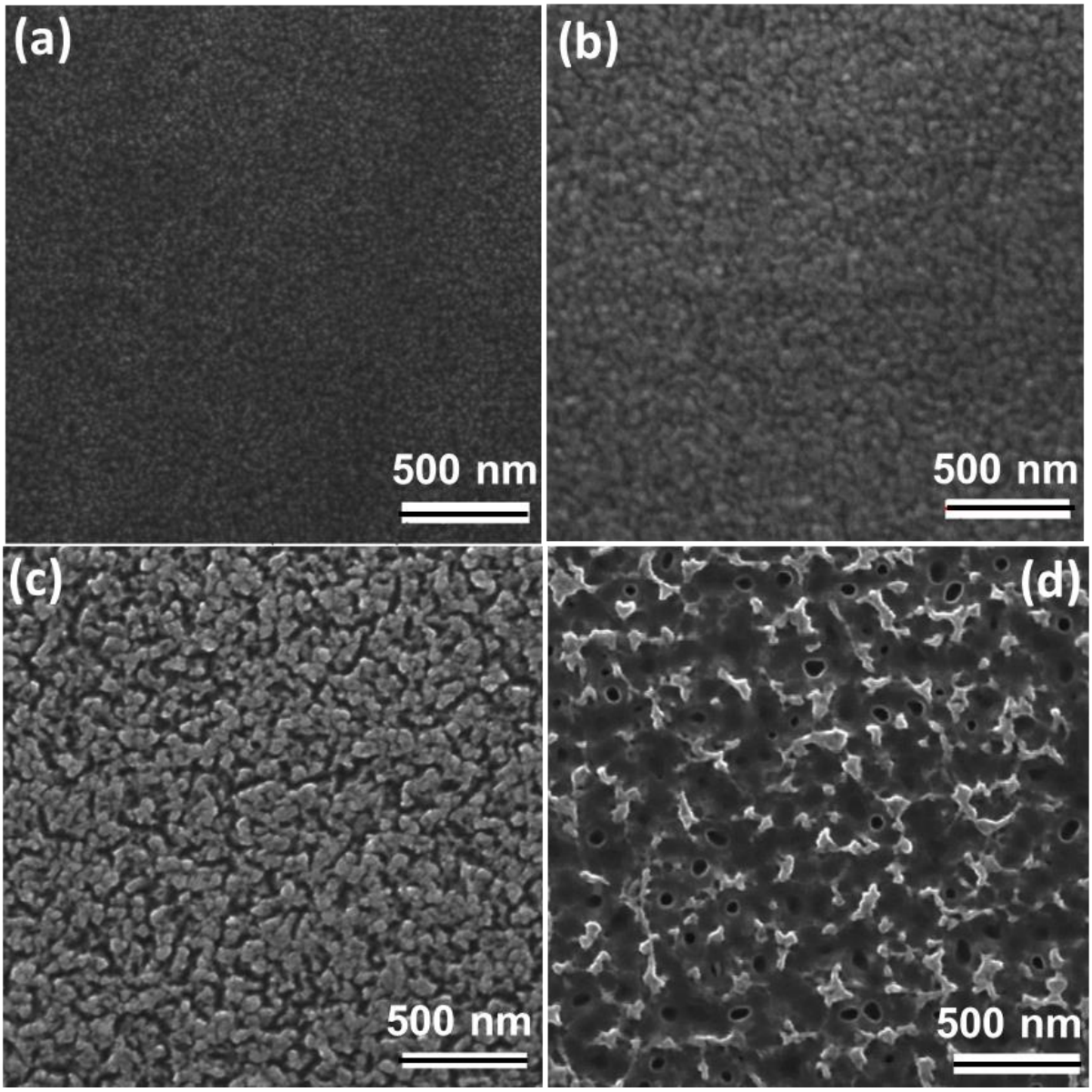

FIG. 3. Saini *et al.*

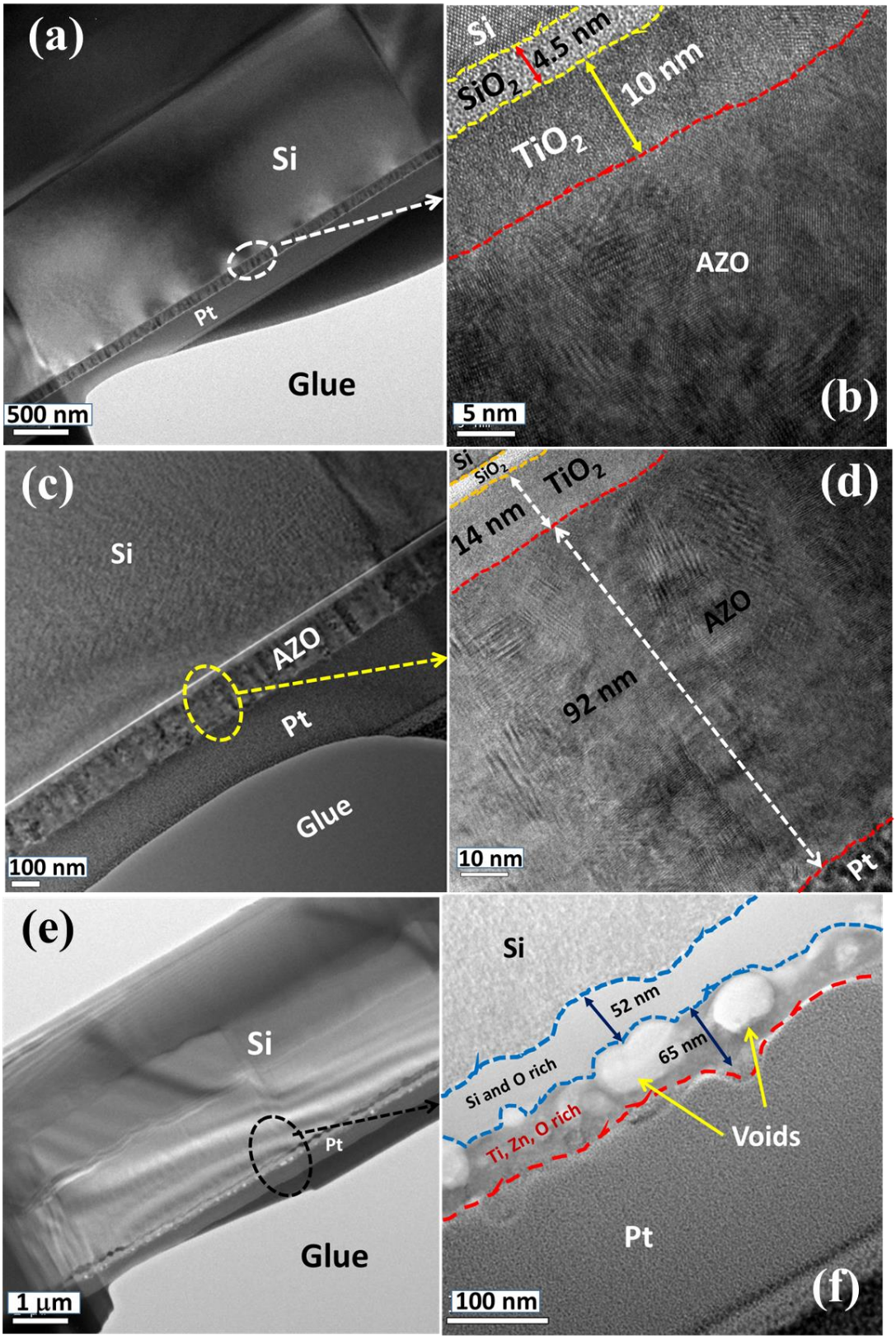

FIG. 4. Saini *et al.*

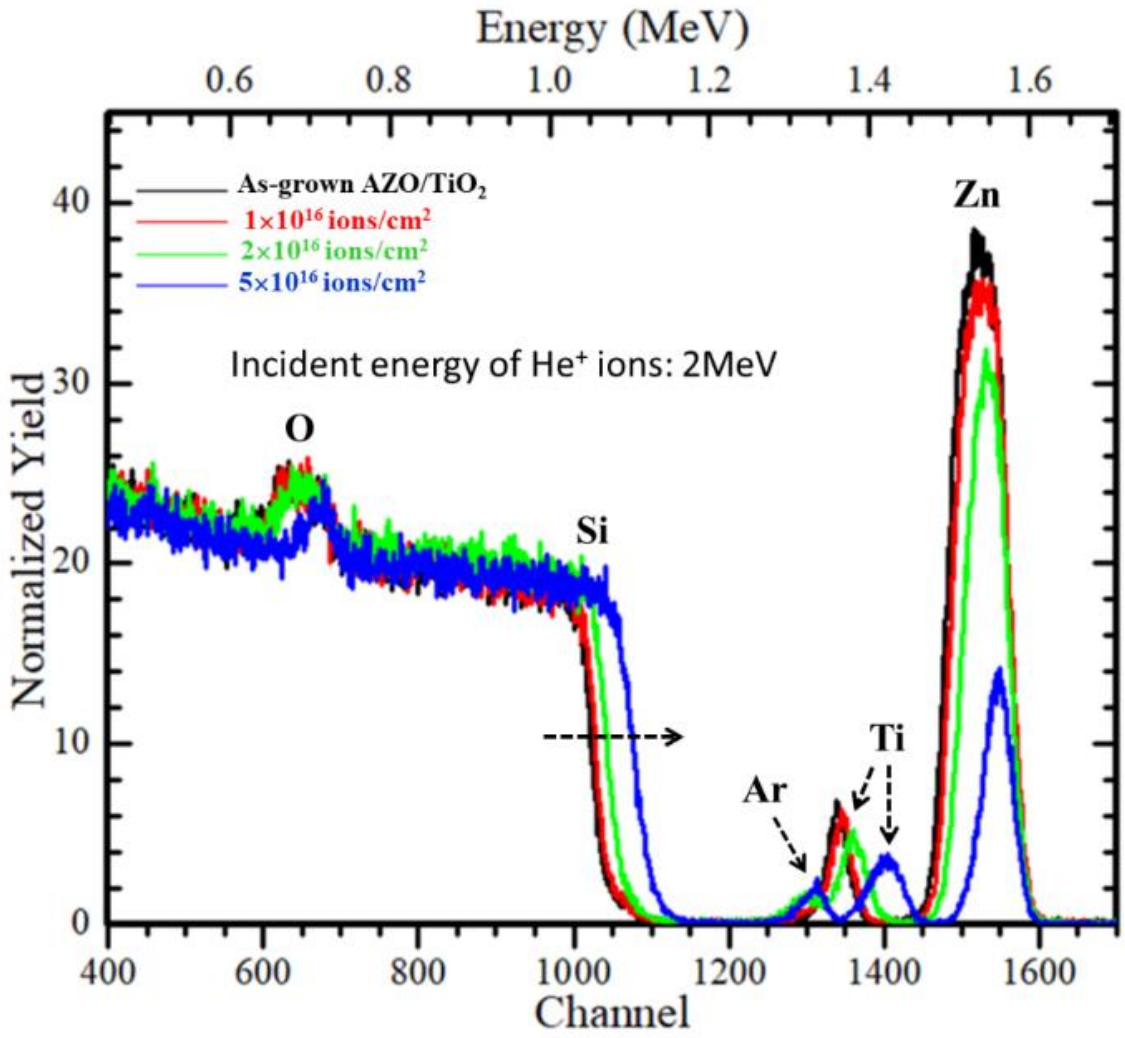

FIG. 5. Saini *et al.*

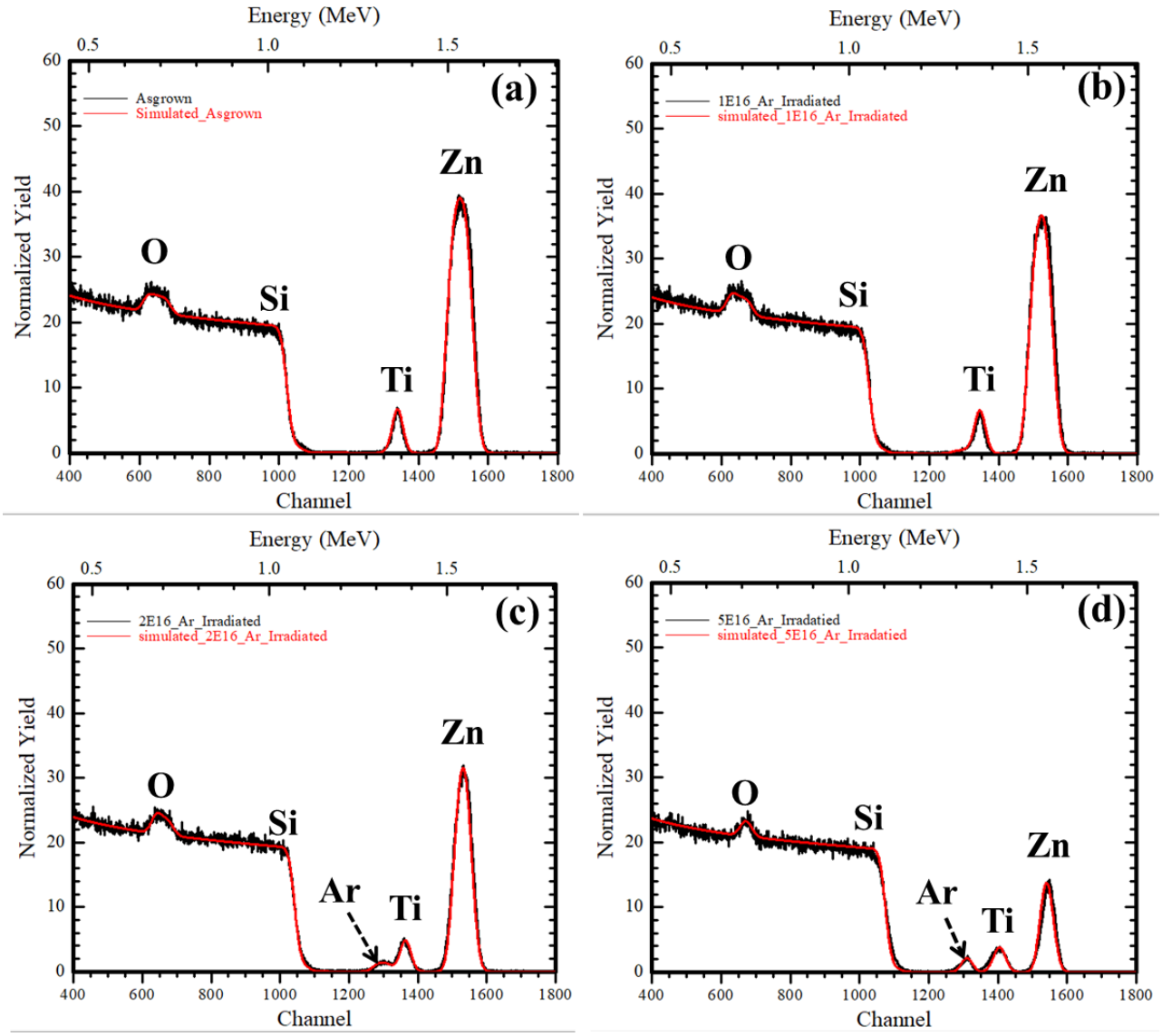

FIG. 6. Saini *et al.*

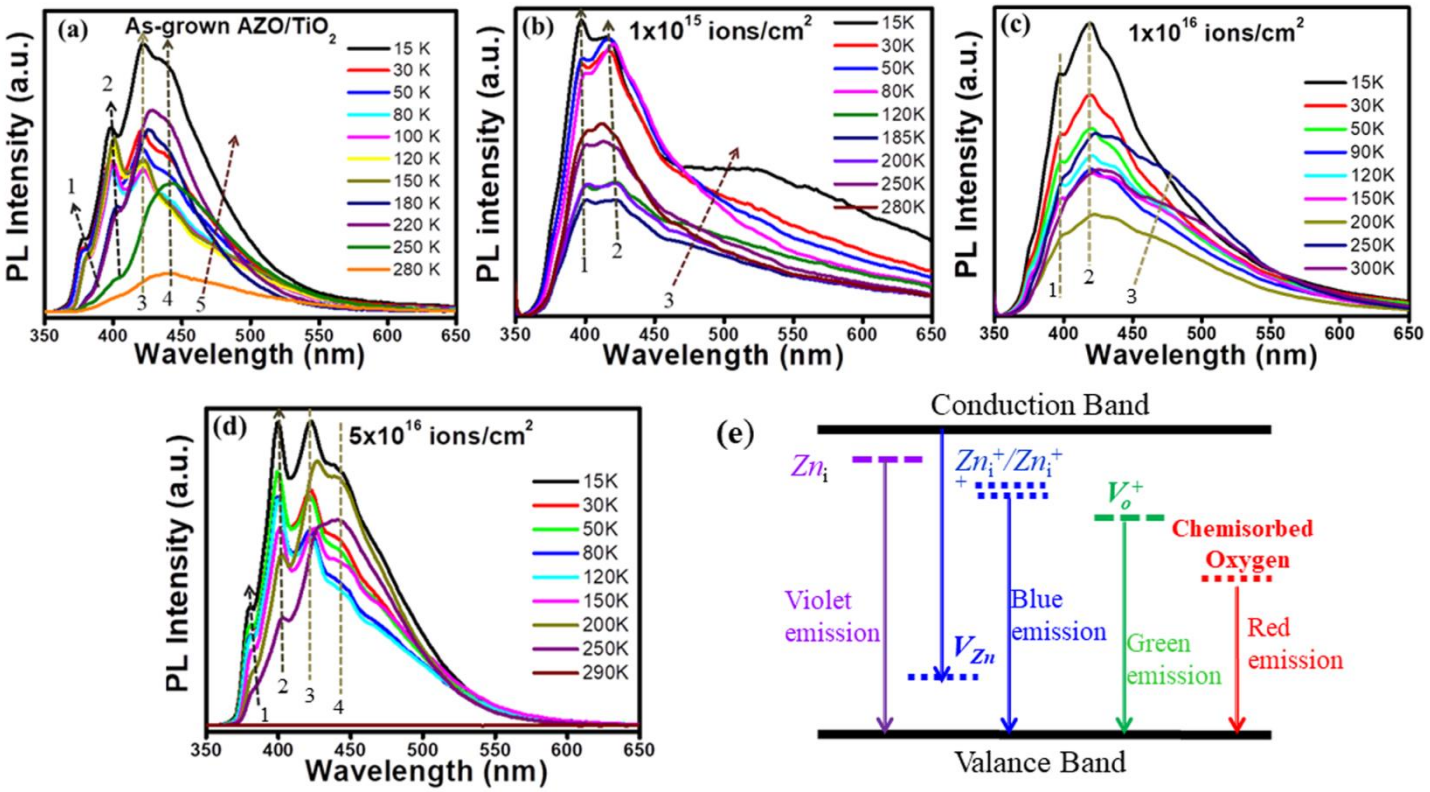

FIG. 7. Saini *et al.*

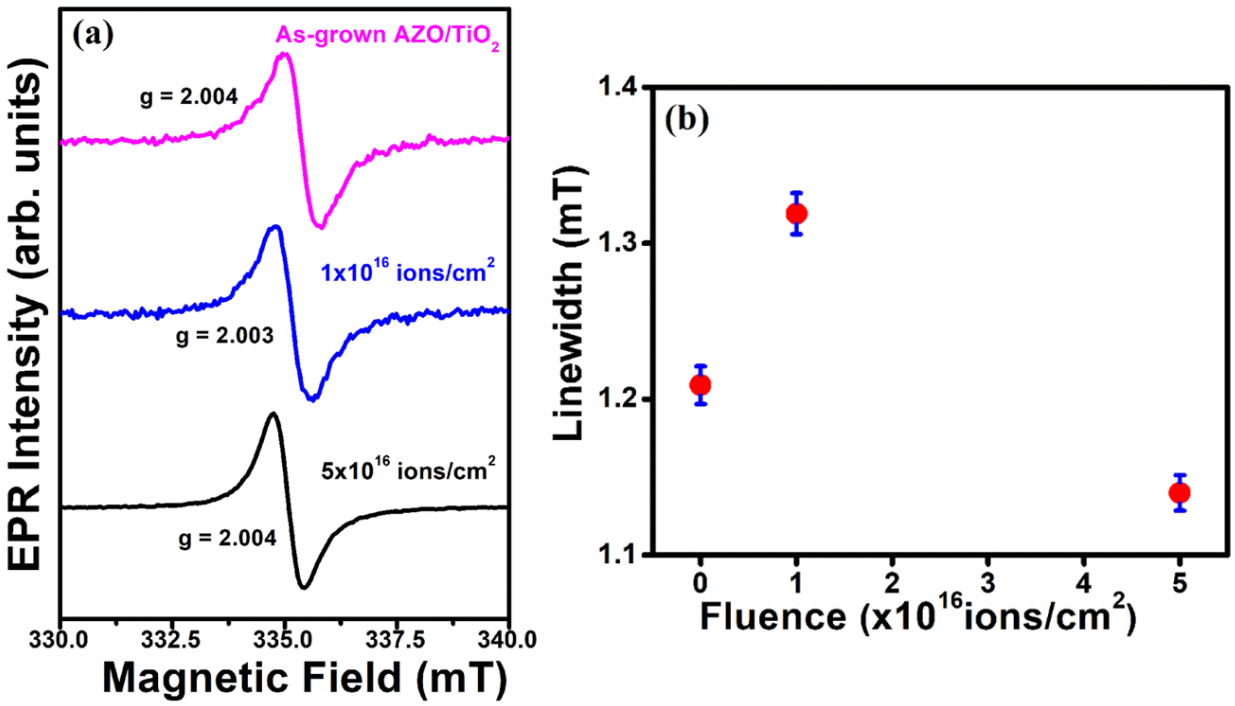

FIG. 8. Saini *et al.*